NUKLEONIKA 2007;52(3):115–123

ORIGINAL PAPER

Radiotracer experiments and CFD simulation for industrial hydrocyclone performance

Zdzisław Stęgowski,
Edward Nowak

Abstract. Hydrocyclone is a device for solid concentration or selection of solid particles from a liquid-solid mixture. It is widely used in the mineral industry for selection of solid particles from a few to a few hundred micrometers. This paper presents a radiotracer experiment and computational simulation of selection of solid particles in a hydrocyclone of Φ-500 mm, which is used in the industrial copper ore concentration process. The simulation, based on computational fluid dynamics (CFD) techniques, allowed obtaining the velocity and concentration distribution for a real mixture flowing in the hydrocyclone. The mixture was composed of water and nine solid phases of different grain sizes. Finally, the selection curve of solid grains was obtained and compared with the experimental radiotracer results.

Key words: computational fluid dynamics • industrial hydrocyclone • selectivity • radioisotope tracer • copper industry

Z. Stęgowski✉, E. Nowak
Faculty of Physics and Applied Computer Science,
AGH University of Science and Technology,
30 A. Mickiewicza Ave., 30-059 Kraków, Poland,
Tel.: +48 12 617 39 15; Fax: +48 12 634 00 10,
E-mail: stegowski@novell.ftj.agh.edu.pl

Received: 12 February 2007
Accepted: 20 July 2007

Introduction

A hydrocyclone is composed of five basic elements which are shown in Fig. 1. The main hydrocyclone vessel is composed of an upper cylindrical element of diameter Φ, and a lower cone element which is characterized by the cone angle α. Tangentially to the cylindrical element, the inlet flow is placed. On the bottom of the cone element there is an open underflow. On the top, in the centre of the cylindrical element, there is an overflow which is connected to a draining pipeline. The overflow is plunged into the cylindrical element. A mixture of water and solid phase enters under pressure the hydrocyclone through the inlet. The tangentially situated inlet generates a circulating flow of the mixture inside the hydrocyclone. For the mixture which flows close to the side walls of the cone parts the circulating flow is combined with a down flow and finally reaches the underflow. In the upper central part of the hydrocyclone, the mixture vertical flow is up and it flows out into the overflow. For solid phase, the centrifugal forces are moving the solid grains to the side walls of the hydrocyclone. The drag forces are counteracted the centrifugal forces. The drag forces depend on grain size and shape and on a turbulent intensity of the flows. For small grains, the centrifugal forces effect is eliminated by drag forces and turbulent diffusion. These grains flow in a similar way to water, so the overflow to underflow flow rate ratio is the same as for water. The centrifugal forces move larger grains to the wall which flow out into the underflow.

The selectivity and classification curves are the basic selection characteristics of the solid particles in a hydro-

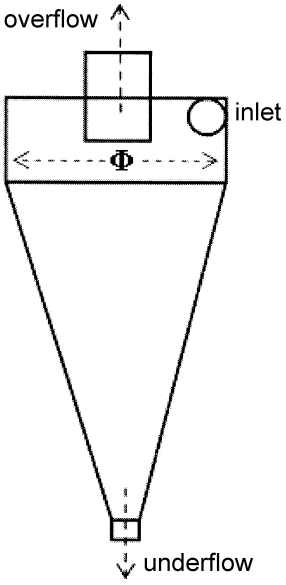

Fig. 1. Design of a hydrocyclone.

cyclone (see Frachon M, Cilliers JJ [10] and Kraipech W *et al*. [11]). The selectivity function $S(d)$ is defined as:

$$S(d) = \frac{U(d)}{F(d)} \tag{1}$$

where $F(d)$ and $U(d)$ are the mass flow rates (kg/s) of particle size d in the feed and the underflow stream, respectively. The classification function $C(d)$ describes selection of particles without small grains which flow in a similar way to water. The relation between $C(d)$ and $S(d)$ is the following:

$$S(d) = C(d) + W\cdot(1 - C(d)) \tag{2}$$

where W is the ratio of mixture flow rate on underflow to mixture feed flow rate.

Figure 2 shows the selectivity and classification curves together with the W ratio. A cut size (d_{50}) parameter is also shown in Fig. 2. The cut size is the major parameter for a hydrocyclone classification process description. The cut size d_{50} is defined as:

$$C(d_{50}) = 0.5 \tag{3}$$

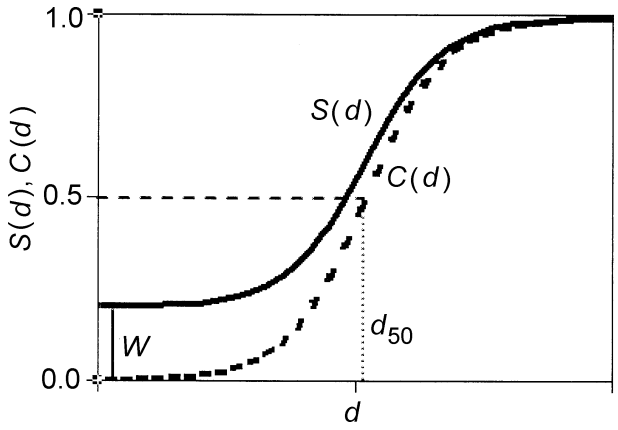

Fig. 2. The selectivity $S(d)$ and classification $C(d)$ curves.

The selectivity function $S(d)$ (in consequence of the $C(d)$ function and W, d_{50} parameters) depends on: hydrocyclone size and geometry, liquid-solid mixture composition and feed flow rate. A lot of experimental results and models for solid particle selection in hydrocyclones have been published. A wide review of these papers was presented by Nageswararao K *et al*. [12] and Dwaria RK *et al*. [7]. Most of the experiments and models concern the evaluation of the cut size d_{50} or the selectivity function $S(d)$. The models are based on the analysis of experimental data. Nageswararao K *et al*. [12] presented such a model for d_{50} evaluation and Frachon M, Cilliers JJ [10] for $S(d)$ evaluation.

In the last decade a significant development in the recognition of liquid-solid mixture flow patterns for a hydrocyclone has been achieved. The first reason of this development is a number of new experimental methods for evaluation of the velocity distribution and the solid phase distribution inside the hydrocyclone. These methods are: laser Doppler velocimetry [4, 6, 9] electrical tomography [2, 8] and ultrasound tomography [17]. The second reason of the emerging development in this field is the application of advanced CFD codes for the flow patterns simulation [5, 13–15, 18, 22, 24].

The paper presents simulation results of flow patterns of a water-solid mixture in the hydrocyclone Φ-500 mm, which is widely used in the industrial copper ore concentration process (see Fig. 3). The "FLUENT" CFD software has been used for the simulations. Finally, the calculated selectivity function $S(d)$ was

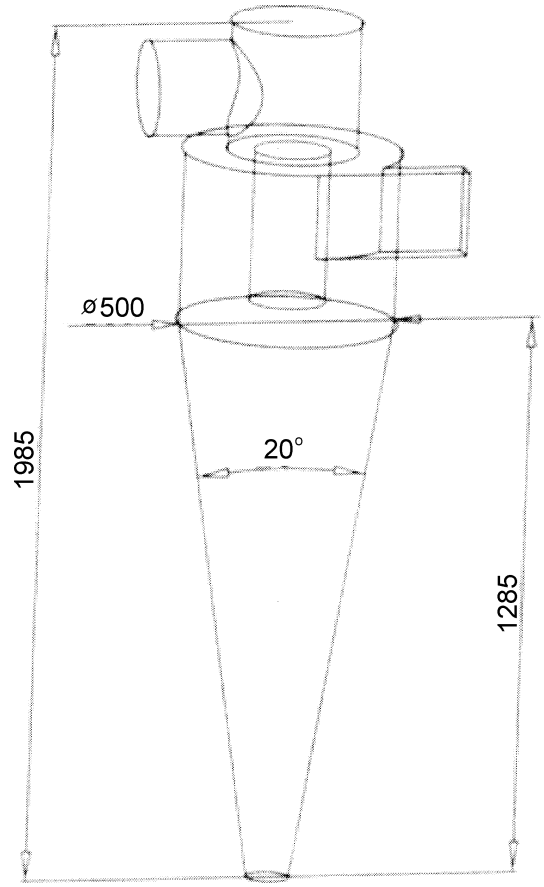

Fig. 3. Schema and dimensions (mm) of the hydrocyclone Φ-500.

compared with the experimental data obtained from an industrial radiotracer experiment.

Industrial radiotracer experiment

The radiotracer method consists in injecting a radioactive tracer into the input of the system and analysis of gamma-radiation intensity distribution (system response) at the output. The possibility of achieving high activity of the tracer per mass unit together with high detection efficiency of gamma-rays allows injection of a small quantity of the tracer in comparison to the flowing material. Thanks to this, the injection does not disturb the process. A properly selected radioisotope, which is naturally associated with the traced population in a flow process, provides information on this population. The method does not influence the process conditions since the detectors measuring the intensity of gamma rays are placed outside the flow. In industrial conditions, particularly in copper ore concentration processes, the radioisotope tracer method is the only one which allows simple, on-line measurements the flow parameters [20].

Radioisotope tracer experiments have been done by injecting labelled, different copper ore grain sizes. The grains were labelled by the radioactive isotope Cu-64 which emits gamma rays of 510 keV energy. The original copper ore samples, for the copper ore process investigation, were activated in nuclear reactor. Amount, of the one sample of copper ore traces, was about 100 g and activity was about 2 GBq. Gamma-ray detectors, the scintillation probes, were placed at the hydrocyclone inlet, underflow outlet and overflow outlet, as shown in Fig. 4. The probes were connected to the computer system for data acquisition and control of experiments. A full description of the radiotracer experiments and other parameters were published in [21]. The detectors measure the gamma-ray intensity which is proportional to the radiotracer activity, to the inverse flow velocity and depend on the measurement point geometry and gamma-ray absorption. The calibration coefficients, allowing to recalculate this intensity to radiotracer activity, were obtained experimentally. This was done by injecting known activities of the radiotracer to the underflow measurement point and measured the gamma-ray intensity. The same was done for the inlet measurement point. For the overflow, this injection was not possible, but the activity balance calculation between inlet, underflow and overflow also allowed to calibrate this measurement point. This method allowed calibrating the experimental distribution curves with accuracy between 5% and 15%. Figure 5 shows the examples of the calibrated experimental time distribution curves $C(t)$ obtained for different particle sizes. The area under each $C(t)$ curve is proportional to the amount of tracer

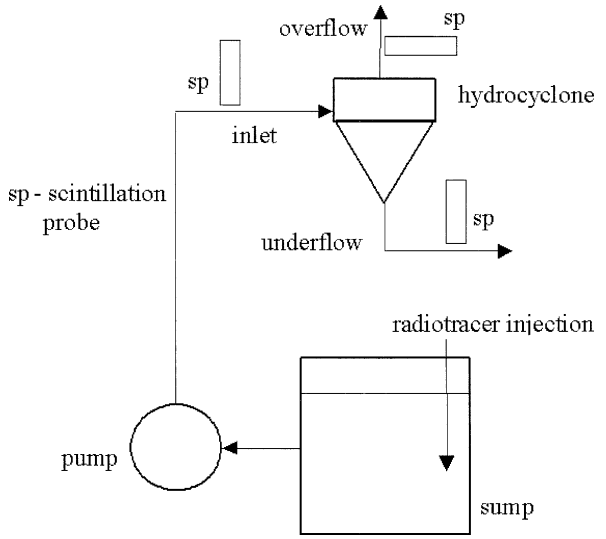

Fig. 4. Schema of the radioisotope tracer experiment.

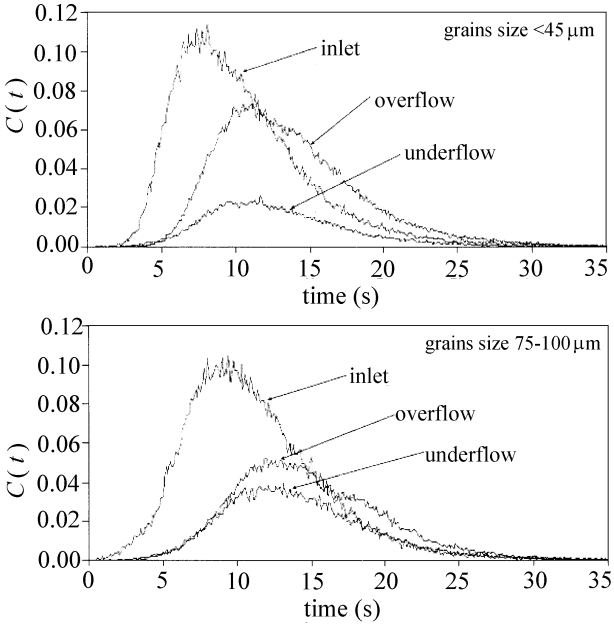

Fig. 5. Calibrated experimental time distribution functions $C(t)$.

passing through the hydrocyclone inlet, underflow and overflow. Finally, the selectivity curve $S(d)$ could be calculated [19]. The obtained results are presented in Table 1.

Mixture flow model theory

The mixture model has been used for simulation of the separation of solid particles in the tested hydrocyclone.

Table 1. Selection coefficients obtained by radiotracer experiments

Grain size (μm)	<45	45–75	75–100	100–150	150–300
Average grain size (μm)	22.5	60	87.5	125	225
Selection coefficient, S	0.26 ± 0.04	0.40 ± 0.04	0.45 ± 0.04	0.70 ± 0.04	0.85 ± 0.04

This model allows to simulate a flow of water (phase $j = 1$) and additional solid phases (phases $j = 2$ to n) of different grain sizes. The mixture model allows the phases to move at different velocities, using the concept of slip velocities. In the hydrocyclone, the slip velocities are consequences of gravitation and centrifugal forces. For turbulence flow, the standard k-ε model has been used. This model is a semi-empirical model, based on model transport equations for the turbulence kinetic energy (k) and its dissipation rate (ε) [16, 23]. The mixture model solves the continuity, momentum, energy equations for the mixture, and the volume fraction equation for the secondary phases, as well as algebraic expressions for the slip velocities. It had been verified that the heat energy production was not significant in this process and the energy equation was not used in the computational modelling. Finally, the following sets of equations were solved:

– the continuity equation for the mixture:

$$\frac{\partial}{\partial t}(\rho_m) + \nabla \cdot (\rho_m \vec{V}_m) = 0 \tag{4}$$

where: $\rho_m = \sum_{j=0}^{n} \alpha_j \rho_j$; $\vec{V}_j = \frac{\sum_{j=0}^{n} \alpha_j \rho_j \vec{V}_j}{\rho_m}$;

j – phase index; α_j – volume fraction of phase j; ρ_j – density of phase j; $\vec{V}_j$ – velocity of phase j.

– the continuity equation for secondary phase ($j > 1$):

$$\partial/\partial t = (\alpha_j \rho_j) + \nabla \cdot (\alpha_j \rho_j \vec{V}_m) = -\nabla \cdot \left(\alpha_j \rho_j (\vec{V}_j - \vec{V}_m)\right) \tag{5}$$

– the momentum equation for the mixture:

$$\frac{\partial}{\partial t}(\rho_m \vec{V}_m) + \nabla (\rho_m \vec{V}_m \vec{V}_m) = -\nabla p + \nabla \cdot \left[\mu_m \left(\nabla \vec{V}_m + \nabla \vec{V}_m^T\right)\right] + \rho_m \vec{g} + \nabla \cdot \left(\sum_{j=1}^{n} \alpha_j \rho_j \left(\vec{V}_j - \vec{V}_m\right)\left(\vec{V}_j - \vec{V}_m\right)\right) \tag{6}$$

where: $\mu_m = \sum_{j=1}^{n} \alpha_j \mu_j$; μ_j – viscosity of phase j.

– the equation for the slip velocity which is defined as the velocity of a secondary phase ($j > 1$) relative to the velocity of the primary phase ($j = 1$):

$$\vec{V}_{j1} = \frac{(\rho_j - \rho_m) d_j^2}{18 \mu_1 f_j} \cdot \left(\vec{g} - (\vec{V}_m \cdot \nabla) \cdot \vec{V}_m - \frac{\partial \vec{V}_m}{\partial t}\right) \tag{7}$$

where: g – acceleration of gravity; d_j – grain size of phase j; f_j – drag function taken from the Schiller and Naumann formula:

$$f_j = \begin{cases} 1 + 0.15 \mathrm{Re}_j^{0.678} & \mathrm{Re}_j \le 1000 \\ 0.0183 \mathrm{Re}_j & \mathrm{R}_j > 1000 \end{cases} \tag{8}$$

where: $\mathrm{Re}_j = [(\rho_1 | \vec{V}_j - \vec{V}_1 | d_j)/\mu_1]$ relative Reynolds number of phase $j > 1$.

– the transport equations of turbulence kinetic energy (k) and its rate of dissipation (ε):

$$\frac{\partial}{\partial t} = (\rho_m k) + \nabla \cdot (\rho_m \vec{V}_m k) = -\nabla \cdot \left(\frac{\mu_{t,m}}{\sigma_k} \cdot \nabla k\right) + G_{k,m} - \rho_m \varepsilon \tag{9}$$

$$\partial/\partial t \cdot (\rho_m \varepsilon) + \nabla \cdot (\rho_m \vec{V}_m \varepsilon) = -\nabla \cdot \left((\mu_{t,m}/\sigma\varepsilon) \cdot \nabla \varepsilon\right) + \varepsilon/k \cdot (C_{1\varepsilon} G_{k,m} - C_{2\varepsilon} \rho_m \varepsilon) \tag{10}$$

where: $\mu_{t,m} = \rho_m C_\mu \cdot (k^2/\varepsilon)$ – turbulent viscosity; $G_{k,m}$ – represents the generation of turbulence kinetic energy calculated from:

$$G_{k,m} = \mu_{t,m} (\nabla \vec{V}_m + (\nabla \vec{V}_m)^T) / \nabla \vec{V}_m \tag{11}$$

The experimental k-ε model constants $C_{1\varepsilon}$, $C_{2\varepsilon}$, C_μ, σ_k and σ_ε have the following values: $C_{1\varepsilon} = 1.44$, $C_{2\varepsilon} = 1.92$, $C_\mu = 0.09$, $\sigma_k = 1.0$, $\sigma_\varepsilon = 1.3$.

Computational modelling results

Conditions of the computing simulation

The Fluent software solves the presented equations using the volume finite elements method [25]. The GAMBIT software was used for the hydrocyclone geometry modelling and mesh generation. The primary calculation allowed optimizing the mesh grid as 220 thousands tetrahedral-hybrid cells. Figure 6 shows the upper part of the meshed hydrocyclone geometry. In the hydrocyclone inlet, a mixture of water and a 9% volume of solid grains was fed. The solid fraction is composed of nine different grain sizes. The solid phase density was 2800 kg/m^3 and the spherical grains had the following diameters: d = 5, 10, 20, 50, 100, 150, 200, 300, 400 µm. The feeding mixture contained 1% volume of each solid grain phase. The achieved feeding mixture density was 1160 kg/m^3 and it was flowing under a pressure of 123,025 Pa. It appeared that the computing simulation for these conditions gave out a stable flow after about 10 thousands iterations. Finally, the fields

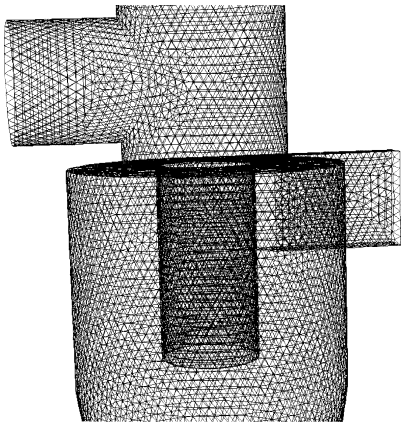

Fig. 6. The upper part of the meshed hydrocyclone geometry.

of velocity, density, pressure, turbulence for the mixture and the fields of velocity and concentration for each solid grain phase have been obtained. These results allowed calculating the average flow parameters and selection of solid grains in the hydrocyclone.

Velocity field

The tangentially placed inlet generates a powerful circulation flow of the mixture inside the hydrocyclone. The circulation velocity is summed with vertical velocity. Near the wall the vertical component of velocity is downward oriented while in the upper-inside part of the hydrocyclone this velocity is upward oriented. Figures 7, 8 and 9 show the examples of the mixture velocity field. Figure 7 shows the circulation velocities on two horizontal cross sections of the cone part of the hydrocyclone. For the same cross sections, the vertical components of velocities are shown in Fig. 8. This figures indicates, that for the whole bottom section the vertical velocity are downward oriented, opposite as for the inside upper section. Figure 9 shows the vertical velocities on the vertical cross section of the hydrocyclone. It can be seen that there are regions where this velocity is upward or downward oriented. Figure 10 shows precisely the region where the vertical velocity is upward

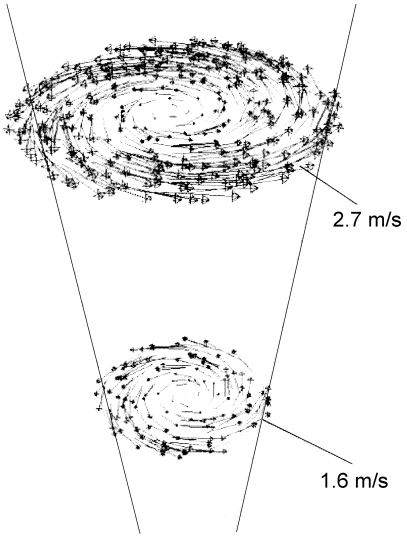

Fig. 7. The circulation mixture velocities on two horizontal cross sections of the cone part of the hydrocyclone.

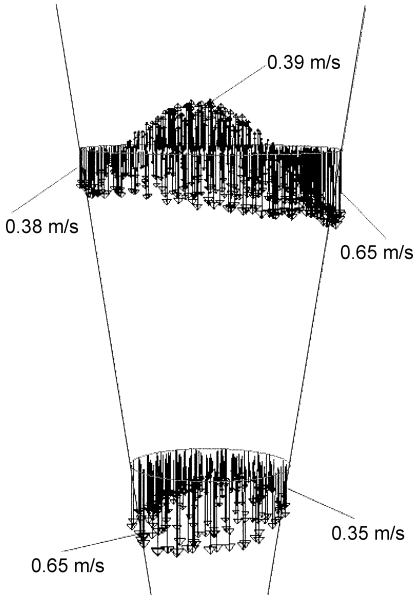

Fig. 8. The vertical components of mixture velocities on two horizontal cross sections of the cone part of the hydrocyclone.

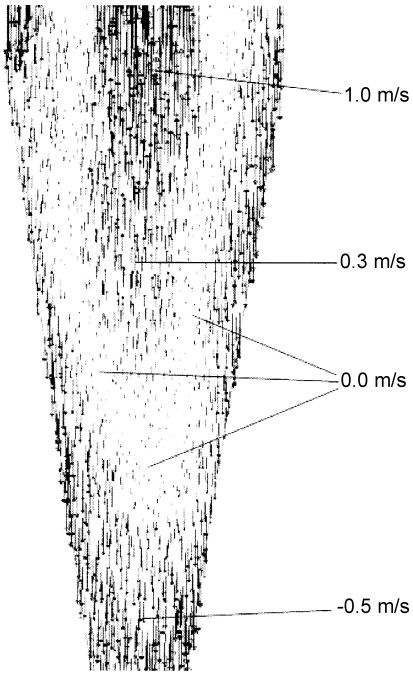

Fig. 9. The vertical mixture velocities on the vertical cross section of the hydrocyclone.

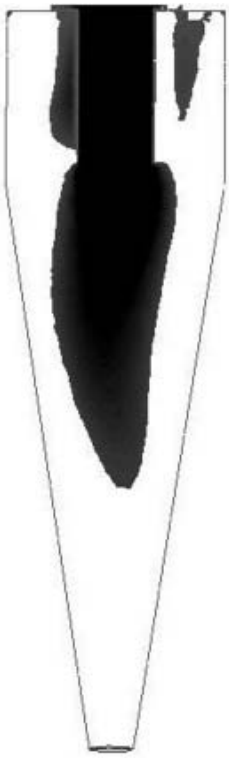

Fig. 10. The region where the vertical velocity is upward oriented.

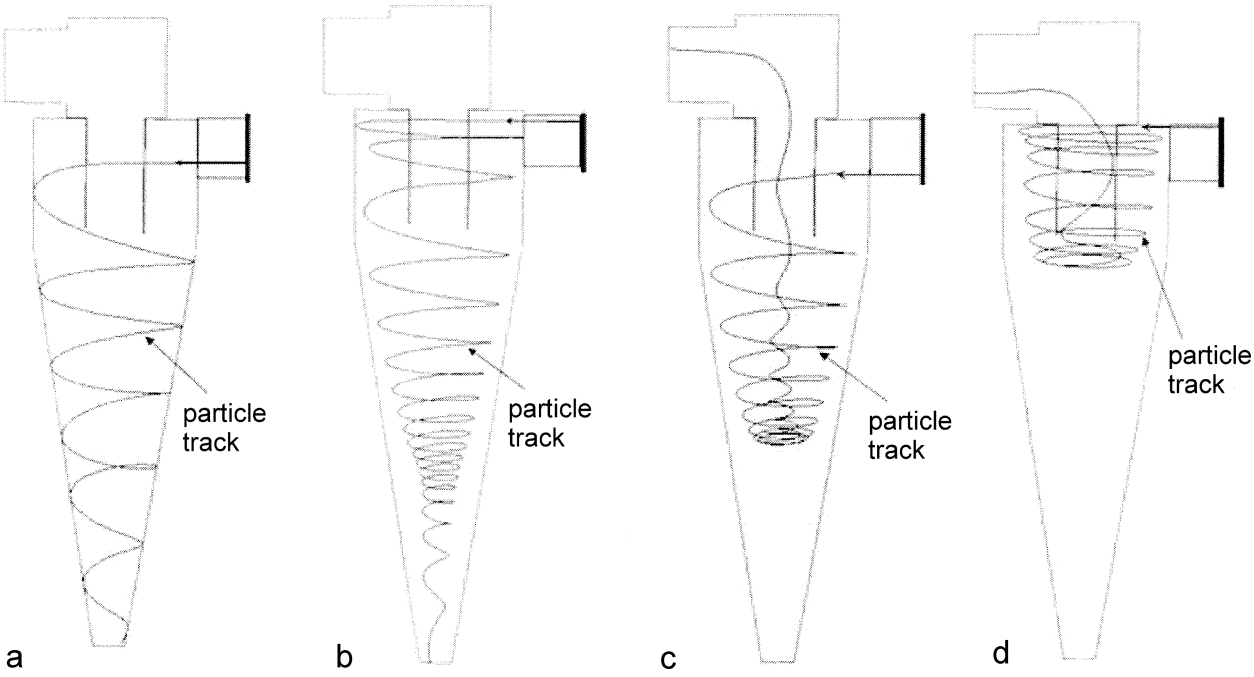

Fig. 11. Water particle tracks.

oriented. Figure 11 shows four examples of water particle tracks. Figure 11a shows the trajectory of the particle which flows close to the wall and after six circulations flows out to the underflow. Figure 11b shows the particle which flows at a small distance to the wall, in the region where the vertical component of velocity is downward oriented, that after eighteen circulations the particle flows out to the underflow. Figures 11c and 11d show the particles that reach the upper flow region and flow out to the overflow.

Concentration distribution

The chapter above presents the mixture velocity field in the hydrocyclone and focuses especially on the regions from which the mixture flows to underflow or to overflow. The selection of solid grains depends on this velocity field and the concentration distribution of solid grains. In the applied model, the centrifugal and gravitation forces generate slip velocity between water and the solid grains what is expressed by Eq. (7). The slip velocity effect causes non-homogeneous concentration of solid grains and the concentration becomes different for different grain sizes. In Fig. 12, the volume water concentration and the volume concentration of solid grain sizes (100 and 300 μm) are shown. Computed results show that big grains (300 and 400 μm) have a high non-homogeneous concentration distribution. These solid grains flow mainly close to the hydrocyclone wall and their maximum concentration, close to the cone wall, varies from 4% to 7% for each grain phase, and 25% for all solid grain phases. On decreasing grain sizes, the concentration changes to homogeneous in the whole volume of the hydrocyclone and for grain sizes smaller than 50 μm it becomes 0.83–1.04%. As expected, close to the cone wall, there is a maximum concentration of big grains and a minimum of small grain (5, 10 and 20 μm). For each solid grain size, the minimum and maximum of the volume concentration, close to the cone wall and to overflow, are presented in Table 2.

Averaging results

Previous chapters presented the mixture velocity field and the concentration distributions of the solid grains that allowed calculating the average values for the entire hydrocyclone volume and for its overflow and underflow. In Table 3, the average values of mixture density for

Table 2. The minimum and maximum of the volume concentration close to the cone wall and to overflow, for each solid grain sizes

Grain sizes (μm)	5	10	20	50	100	150	200	300	400
C_V (%) close the wall	0.83	0.84	0.87	1.13	1.8	2.7	3.8	5.6	7.0
C_V (%) in overflow	1.04	1.04	1.03	0.7	0.28	0.09	0.03	0.002	0.002

Table 3. Average values of mixture density for the inlet, overflow, underflow and the whole volume

	Inlet	Overflow	Underflow	Volume
Average density values (kg/m^3)	1160	1098	1280	1149

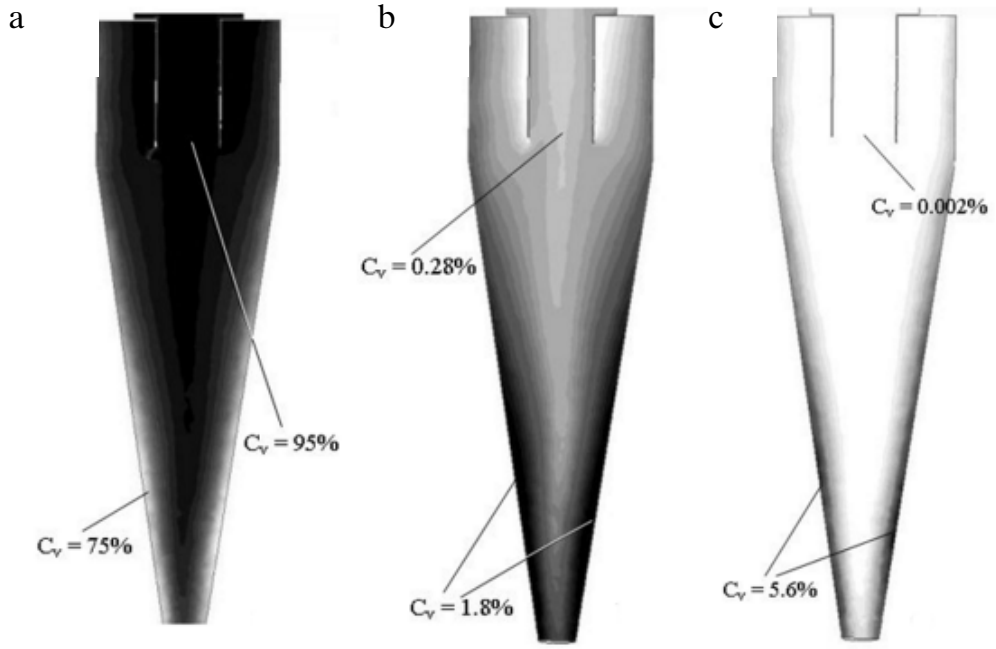

Fig. 12. Volume concentration of (a) water, (b) solid grain sizes 100 μm, (c) solid grain sizes 300 μm.

the inlet, overflow, underflow and the whole volume are presented. The average values of volume concentration of water and each solid grain size are presented in Table 4. The large difference in the density between the overflow (1098 kg/m^3) and the underflow (1280 kg/m^3) is a result of the concentration distribution of big grains which is the largest in the downward flowing region of the hydrocyclone. The grain sizes smaller than 50 μm have a homogeneous concentration distribution and they are flowing in a similar way to water. The average volume concentration of the big grain sizes is smaller than 1%, in consequence, the average volume density of the mixture (1149 kg/m^3) is smaller than the feed mixture density (1160 kg/m^3). It could be concluded that the bigger grains have a smaller mean residence time (MRT) in relation to the other phases of the mixture. The compute simulations of single particle flow trajectories proved this conclusion. For each phase of the mixture, the flow trajectory of 500 particles was simulated and the MRT calculated. The MRT values are presented in Table 5.

Flow rates of the solid phases allow obtaining the selectivity function according to Eq. (1). The mass flow rates for the mixture, water and solid grain phases are

Table 4. Average values of volume concentration of water and of each solid grain size

	Average volume fraction (%)			
	inlet	overflow	underflow	volume
Solid (μm)				
5	1.00	1.04	0.93	1.00
10	1.00	1.03	0.94	1.00
20	1.00	1.02	0.96	1.00
50	1.00	0.94	1.11	1.00
100	1.00	0.71	1.55	0.98
150	1.00	0.46	2.03	0.95
200	1.00	0.26	2.41	0.90
300	1.00	0.07	2.79	0.80
400	1.00	0.02	5.43	0.74
Water	91.0	94.4	84.4	91.61

Table 5. Simulated data of the mean residence time (MRT)

	Grain sizes (μm)									
	Water	5	10	20	50	100	150	200	300	400
MRT (s) underflow	4.52	4.56	4.54	4.53	4.26	3.95	3.50	3.36	3.22	3.15
MRT (s) overflow	4.57	4.18	4.14	4.13	4.17	3.76	3.70	3.41	–	–

Table 6. The mass flow rates for the mixture, water and solid grain phases

	Mass flow rate (kg/s)		
	inlet	overflow	underflow
Mixture	37.1	25.8	11.3
Water	33.7	24.4	9.3
Solid (μm)			
5	0.37	0.27	0.10
10	0.37	0.27	0.10
20	0.37	0.26	0.11
50	0.37	0.24	0.13
100	0.37	0.19	0.18
150	0.37	0.12	0.25
200	0.37	0.07	0.30
300	0.37	0.018	0.352
400	0.37	0.004	0.366

presented in Table 6. A comparison of these data with the experimental results are presented and discussed in the next chapter.

Summary of results

The simulation has been performed for the conditions similar to those encountered during the industrial radiotracer experiments. The hydrocyclone geometry, mixture density, solid density and inlet pressure were the same in both cases. In industrial conditions the solid grain sizes distribution was continuous. During simulation, for the software and computer limits, this distribution was discrete and it was composed of nine grain sizes of the solid phase. On the basis of experimental results (Table 1) and computer simulated data (Table 6), the proper selectivity functions were derived. They are shown in Fig. 13. This figure shows that the experimental and computed results are compatible. For computed results, the value of W parameter (Eq. (2)) is 0.27 and for the experimental results it is between 0.25–0.26. The cut size d_{50} (Eq. (3)) is approximately 170 μm for both results.

These results allow to state the thesis that the applied model and the computer simulation sufficiently describe the flow pattern of the water-solid mixture in a hydrocyclone. Then, accepting this thesis, two further conclusions can be drawn. The first conclusion is: prediction of the separation of solid grains for the specified hydrocyclone geometry and feed flow parameters is possible. In consequence, the computer simulation could become a main stage of the hydrocyclone separation process design. The second conclusion concerns the physical pattern of the water-solid mixture flow in a hydrocyclone. It means that the circulation mixture flow is strongly constrained and for the bigger grain sizes the turbulence diffusion and the grain interaction could be omitted. For these grains, the slip velocity effect for the concentration distribution is dominated.

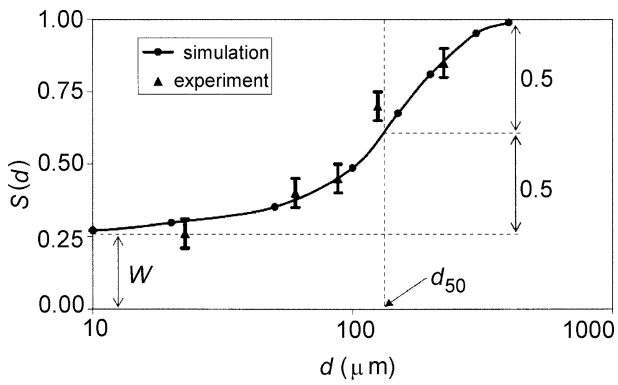

Fig. 13. The experimental and simulation selectivity functions.

Conclusion

In the last decade a significant development in the experimental abilities and the computer simulation have been achieved for recognition of liquid-solid mixture flow patterns in hydrocyclones, as it has been presented in the introduction chapter. The advances in available computational power and progress in development of numerical codes have enhanced calculation possibilities for the new models.

The available computer facility allowed the simulating water-solid mixture flow for nine phases of solid particles, using the k-ε turbulence flow model and 220 thousands mesh grid for the hydrocyclone. The Fluent software enables to use turbulence flow models like: Reynolds-Stress and Large Eddy Simulation models, but they need more computational power. Application of these models and the comparison of their results would be valuable.

For the solid particles, the selection process in a hydrocyclone and the experimental measurement of the particle tracks would be valuable for the assumed model and its computational validation of results. Bhusarapu S *et al.* [3] have described the radiotracer method for particle track measurements. The radiotracer methods are not widely used in chemical engineering investigations. The possibilities of these methods for industrial applications are presented by Axelsson G *et al.* [1].

The water-solid mixture flow in a hydrocyclone is a complex physical process for theoretical description and, in consequence, for computational simulation. Nearly each model has theoretical or computational limitations, e.g. some physical effects are difficult for mathematical modelling or computational calculation. For mathematical modelling of the turbulent mixture flow, some experimental relations and parameters are used.

As the physical phenomena, which are enough precisely described in the model, are prevailed in the described process then the model can be applied in practise. It could be possible that the presented model and its computational results is a kind of practicability model for the selection of solid particles in hydrocyclone.

Notation

$C(d)$ – classification function
$C(t)$ – calibrated experimental time distribution curve
$C_{1\varepsilon}$ – experimental constant
$C_{2\varepsilon}$ – experimental constant
C_{μ} – experimental constant
d – particle size, mm
d_j – grain size of phase j, mm
d_{50} – cut size, mm
f_j – drag function
F – feed mass flow rates, kg/s
g – acceleration of gravity, m/s^2
$G_{k,m}$ – generation of turbulence kinetic energy, kg/m·s^3
j – phase index
k – turbulence kinetic energy, m^2/s^2
Re – Reynolds number
S – selectivity function
t – time, s
U – underflow mass flow rates, kg/s
$\vec{V}_j$ – velocity of phase j, m/s
$\vec{V}_m$ – mixture velocity, m/s
W – ratio of water flow rate

Greek letters

α_j – volume fraction of phase j
ε – turbulence kinetic energy dissipation, m^2/s^3
μ_j – viscosity of phase j, kg/m·s
μ_m – mixture viscosity, kg/m·s
$\mu_{t,m}$ – turbulent viscosity, kg/m·s
ρ_j – density of phase j, kg/m^3
σ_ε – experimental constant
σ_k – experimental constant
ρ_m – mixture density, kg/m^3

Acknowledgment. The authors gratefully acknowledge financial support of the Ministry of Scientific Research and Information Technology.

References

1. Axelsson G, Barry BJ, Berne P *et al*. (2004) Radiotracer application in industry – a guidebook. International Atomic Energy Agency, Vienna
2. Bennett MA, Williams RA (2004) Monitoring the operation of an oil/water separator using impedance tomography. Miner Eng 17:605–614
3. Bhusarapu S, Al-Dahhan M, Dudukovic MP (2004) Quantification of solids flow in a gas-solid riser: single radioactive particle tracking. Chem Eng Sci 59:5381–5386
4. Chiné B, Concha F (2000) Flow patterns in conical and cylindrical hydrocyclones. Chem Eng J 80:267–273
5. Cullivan JC, Williams RA, Dyakowski T, Cross CR (2004) New understanding of a hydrocyclone flow field and separation mechanism from computational fluid dynamics. Miner Eng 17:651–660
6. Dai GQ, Chen WM, Li JM, Chu LY (1999) Experimental study of solid-liquid two-phase flow in a hydrocyclone. Chem Eng J 74:211–216
7. Dwaria RK, Biswasb MN, Meikapa BC (2004) Performance characteristics for particles of sand FCC and fly ash in a novel hydrocyclone. Chem Eng Sci 59:671–684
8. Dyakowski T, Jeanmer LFC, Jaworski AJ (2000) Applications of electrical tomography for gas-solids and liquid-solids flow – a review. Powder Technol 112:174–192
9. Fisher MJ, Flack RD (2002) Velocity distributions in a hydrocyclone separator. Exp Fluids 32:302–312
10. Frachon M, Cilliers JJ (1999) A general model for hydrocyclone partition curves. Chem Eng J 73:53–59
11. Kraipech W, Chen W, Parma FJ, Dyakowski T (2002) Modelling the fish-hook effect of the flow within hydrocyclones. Int J Miner Process 66:49–65
12. Nageswararao K, Wiseman DM, Napier-Munn TJ (2004) Two empirical hydrocyclone models revisited. Miner Eng 17:671–687
13. Narasimha M, Sripriya R, Banerjee PK (2005) CFD modelling of hydrocyclone – prediction of cut size. Int J Miner Process 75:53–68
14. Nowakowski AF, Cullivan JC, Williams RA, Dyakowski T (2004) Application of CFD to modelling of the flow in hydrocyclones. Is this a realizable option or still a research challenge? Miner Eng 17:661–669
15. Olson TJ, Van Ommen R (2004) Optimizing hydrocyclone design using advanced CFD model. Miner Eng 17:713–720
16. Pope BS (2000) Turbulent flow. Cambridge University Press, Cambridge, UK
17. Schlaberg HS, Frank Podd FJW, Hoyle BS (2000) Ultrasound process tomography system for hydrocyclones. Ultrason 38:813–816
18. Slack MD, Del Porte S, Engelman MS (2004) Designing automated computational fluid dynamics modeling tools for hydrocyclone design. Miner Eng 17:705–711
19. Stęgowski Z (1993) Accuracy of residence time distribution function parameters. Nucl Geophys 7;2:335–341
20. Stęgowski Z, Furman L (2004) Radioisotope tracer investigation and modeling of copper concentrate dewatering process. Int J Miner Process 73:37–43
21. Stęgowski Z, Leclerc J-P (2002) Determination of the solid separation and residence time distributions in an industrial hydrocyclone using radioisotope tracer experiments. Int J Miner Process 66:67–77
22. Stęgowski Z, Nowak E, Furman L (2004) Combining CFD simulation with experimental RTD funcion for hydrocyclone separator studies. In: Integration of tracing with computational fluid dynamics for industrial process investigation. International Atomic Energy Agency, Vienna. IAEA-TECDOC-1412, pp 161–178
23. Wilkes JO (1999) Fluid mechanics for chemical engineers. Prentice Hall PTR, Upper Saddle River, New Jersey
24. Yang IH, Shin CB, Kim T-H, Kim S (2004) A three-dimensional simulation of a hydrocyclone for the sludge separation in water purifying plants and comparison with experimental data. Miner Eng 17:637–641
25. Zbeng Ch, Bennet GD (2002) Applied contaminant transport modeling. John Wiley and Sons, New York